The Geometry of Separation Boundaries: Four-Component Mixtures

Meghan Bellows and Angelo Lucia
Dept. of Chemical Engineering, University of Rhode Island, Kingston, RI 02881

DOI 10.1002/aic.11187
Published online May 7, 2007 in Wiley InterScience (www.interscience.wiley.com).

The determination of distillation boundaries for four-component mixtures that exhibit azeotropy is studied. It is shown that these distillation boundaries correspond to local maxima in surface areas under conditions of Levi-Civita parallelism. An extension of the optimization methodology given in Lucia and Taylor is used to determine local maxima in surface areas by repeatedly computing maximum line integrals or distances in one spherical coordinate over a set of initial conditions that span the range of the second spherical coordinate. An optimization formulation that defines the determination of local maxima in surface areas subject to residue curve and stable node constraints is given. Numerical measurement of surface areas is accomplished using a triangulation procedure. Several numerical examples of varying complexity involving four-component mixtures that exhibit azeotropes are presented to show the efficacy of the proposed optimization methodology. Geometric illustrations are used throughout to highlight key features of our methodology for determining distillation boundaries in four-component mixtures. © 2007 American Institute of Chemical Engineers *AIChE J,* 53: 1770–1778, 2007

Keywords: distillation boundaries, four-component mixtures, surface areas, Levi-Civita parallelism

Introduction

Residue curves, originally proposed by Ostwald[1,2] and Schreinemakers,[3–5] are an important tool in distillation design—especially when the mixture to be separated is azeotropic. The presence of azeotropes increases the complexity of any separation by giving rise to distillation boundaries. Residue curves can be used to guide understanding and to help identify those separations that are possible by distillation in the face of these boundaries.

A residue curve is simply a trajectory that describes the composition changes of liquid residue as it is boiled in an open pot and the vapor formed is removed immediately. When different charges to this open pot or starting compositions are boiled they yield different residue curves, and any collection of residue curves is called a residue curve map. Residue curves are analogous to packed distillation towers operated at total reflux, and are generated by solving a set of nonlinear differential equations of the form.

$$x' = y - x \tag{1}$$

where y is a $(c - 1)$ vector of mole fractions in the vapor phase, x is a $(c - 1)$ vector of liquid mole fractions, x' is the change in the mole fractions in the liquid phase, and c is the number of components. Residue curves given by Eq. 1 flow from high temperature to low temperature and an important physical feature that affects the behavior of these trajectories for azeotropic mixtures is the presence of distillation boundaries. These boundaries divide the feasible region into distillation regions that, in general, cannot be crossed using conventional distillation. Thus, knowledge of the location and shape of these boundaries is important in distillation design.

Recently, Lucia and Taylor[6] showed that for ternary mixtures distillation boundaries are defined by the locally longest

Correspondence concerning this article should be addressed to A. Lucia at lucia@egr.uri.edu.

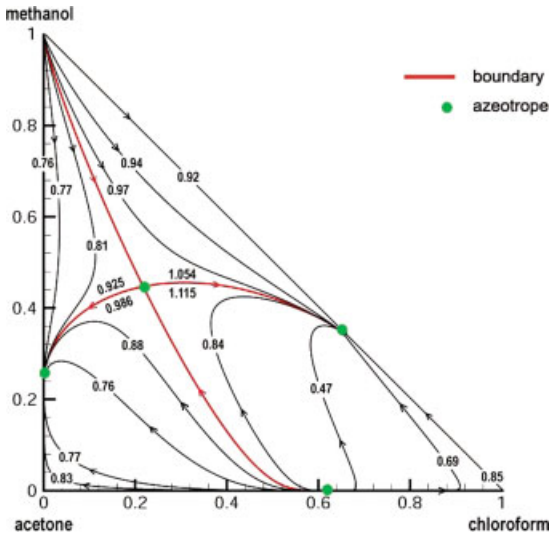

Figure 1. Residue curve map and line integrals for chloroform/methanol/acetone.

[Color figure can be viewed in the online issue, which is available at www.interscience.wiley.com.]

trajectories (or local maxima in line integral) from any unstable to any reachable stable node of Eq. 1. Figure 1 gives an illustration of this concept of distillation boundaries being local maxima in line integrals or distance for the system chloroform, methanol, and acetone at atmospheric pressure. This mixture has three binary azeotropes and one ternary azeotrope and separates the composition triangle into four distinct distillation regions. Note, however, that the boundaries correspond to the longest trajectories in any given region.

In their article, Lucia and Taylor also described an extension of the geometric concept of maximum distance for ternary systems to maximum surface areas for four-component mixtures, such that distillation boundaries are given by the solution to the following mathematical programming problem.

$$\max_{x(0)} A = \iint [x'(\alpha_1, \alpha_2)] d\alpha_1 \, d\alpha_2 \tag{2}$$

$$\text{subject to} \quad x'(\alpha_1, \alpha_2) = y[x'(\alpha_1, \alpha_2)] - x(\alpha_1, \alpha_2) \tag{3}$$

$$x(T) = x_T \tag{4}$$

where A is the surface area, $x(\alpha_1, \alpha_2)$ is parameterization of any trajectory over the domain of interest, $\| \cdot \|$ denotes the two-norm, $x(0)$ is any feasible set of initial conditions on the ball of radius ε about some designated unstable node x_0, and x_T is a stable node, and where the ball of radius ε about a designated unstable node x_0 is defined by $B(x_0, \varepsilon) = \{x: \| x - x_0 \| = \varepsilon \text{ for all } x\}$. Unfortunately, Lucia and Taylor do not give any details regarding the conditions under which Eqs. 2–4 hold or how the problem defined by Eqs. 2 through 4 can actually be solved.

The purpose of this article is to pursue the remarks in Lucia and Taylor[6] and describe in detail a methodology that extends the concept of maximum line integrals to mixtures of four components. Accordingly, this paper is organized in the following way. First, we provide a brief survey of the relevant literature. The geometric ideas of Lucia and Taylor are summarized and then extended to four-component mixtures. In particular, a triangulation procedure is described for calculating surface areas, and Levi-Civita parallelism is used to provide meaningful comparisons of surface areas. Next, an optimization formulation for finding distillation boundaries in four-component mixtures is presented. Following that, numerical results for a number of examples are given, and our results are then summarized.

Brief Literature Survey

The literature on residue curves is extensive. However, only the literature that is relevant to the material presented in this article is discussed here. For a more comprehensive literature survey, the reader is referred to the article by Kiva et al.[7]

Most of the literature for residue curve maps and distillation boundaries is restricted to three-component mixtures. Only a few articles discuss related ideas for mixtures with four or more components. The first papers on residue curves are those of Ostwald[1,2] and Schreinemakers[3–5] in 1901, while the work of Doherty and Perkins[8] has led to our current knowledge of residue curves and distillation boundaries. This work has been further developed by Doherty and coworkers as it applies to homogeneous mixtures,[9] heterogeneous mixtures,[10,11] and reactive mixtures.[12–14] Van Dongen and Doherty[15] showed that simple boundaries do not coincide with the ridges and valleys of any boiling temperature surfaces as was previously thought. Nevertheless, a variety of authors have contributed to the development of numerical procedures for computing approximate separation boundaries, including Foucher et al.,[16] Peterson and Partin,[17] and Rooks et al.[18] Recently Krolikowski[19] has used a bifurcation study for a single-feed column to determine distillation boundaries. Finally, the work of Pöpken and Gmehling[20] extended the ideas of Rooks et al. to four-component systems. Despite a large body of work, there existed no clear definition or simple methodology for computing exact distillation boundaries—at least until the work of Lucia and Taylor.[6]

Background

Before discussing the geometric concepts associated with quaternary mixtures, we give a very brief summary of the work of Lucia and Taylor[6] for ternary mixtures. A separation boundary is any trajectory, say $x^*(\alpha)$, associated with the solution of the nonlinear programming problem.

$$\max_{x(0)} D = \int_0^T \|x'(\alpha)\| d\alpha \tag{5}$$

$$\text{subject to} \quad x'(\alpha) = y[x(\alpha)] - x(\alpha) \tag{6}$$

$$x(T) = x_T \tag{7}$$

where D represents a line integral or distance function along a trajectory, $\| \cdot \|$ denotes the two-norm, $x(0)$ is any feasible

set of initial conditions on the circle of radius ε about some designated unstable node, x_0, and x_T is a stable node. Note that the objective function, D, in Eq. 5 is only a function of the initial conditions, $x(0)$, which are the unknown optimization variables, and any trajectory, $x^*(\alpha)$, that corresponds to a local maximum value of distance is a separation boundary. Also, it is implied that all azeotropic compositions and temperatures of a given mixture have been determined prior to solving Eqs. 5–7.

To find any boundary in a ternary mixture, we proceed as follows. Given an initial set of feasible initial conditions, $x(0)$, defined on $B(x_0, \varepsilon)$, we integrate Eq. 6 and determine the distance along the resulting trajectory. Since each trajectory is uniquely defined by initial conditions, this distance is, as noted, only a function of the initial conditions. In polar coordinates, this fact results in a single degree of freedom for any ternary mixture, because $x(0)$ is related to both the radius, ε, and an angle of rotation, θ, through the simple relationship $x(0) = x_0 + \varepsilon[\cos\theta, \sin\theta]$. Thus D is only a function of θ for fixed ε, and by using optimization to adjust the initial conditions on $B(x_0, \varepsilon)$ in an intelligent way, we can maximize this distance. The resulting trajectory of maximum distance, $x^*(\alpha)$, is a distillation boundary.

Surface Areas and Boundaries in Four-Component Mixtures

The feasible region of a four-component mixture is a tetrahedron, while each of the four triangular faces of the tetrahedron represent the feasible region of the appropriate three-component mixture. In order to introduce the reader to the fundamental geometric concepts of boundaries in quaternary mixtures studied in this work, we start with an illustration. Figure 2 shows the azeotropes, distillation boundaries, trajectories on the boundary surfaces, and surface areas of one boundary as well as a separate collection of trajectories that form an interior surface for the four-component mixture of methanol, ethanol, acetone, and water at atmospheric pressure.

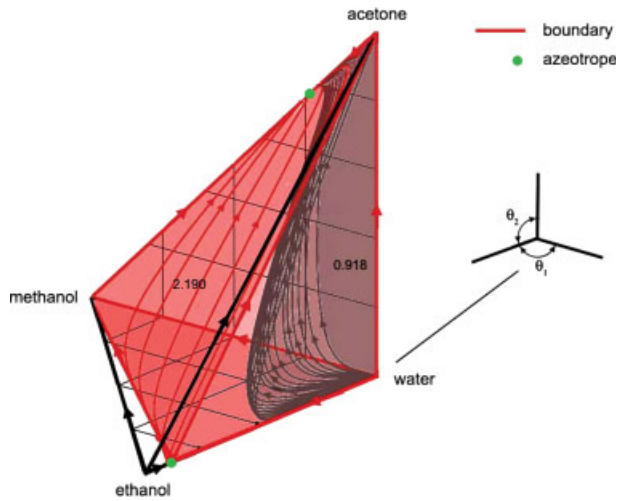

Figure 2. A simple illustration of surface areas and distillation boundaries.

[Color figure can be viewed in the online issue, which is available at www.interscience.wiley.com.]

Table 1. Upper and Lower Bounds on θ_1, θ_2 and z_1, z_2

Node	θ_1	z_1	θ_2	z_2
(0, 0, 0)	[0, π/2]	[0, 1]	[0, π/2]	[0, 1]
(1, 0, 0)	[3π/4, π]	[1.5, 2]	[π/4, π/2]	[0.5, 1]
(0, 1, 0)	[3π/2, 7π/4]	[3, 3.5]	[π/4, π/2]	[0.5, 1]
(0, 0, 1)	[0, π/2]	[0, 1]	[3π/4, π]	[1.5, 2]

It is important to understand that the trajectories shown in Figure 2 lie in the appropriate surfaces shown in that figure. That is, all of the trajectories shown in red are actually contained in the red boundary surface while those in black are contained in the smaller interior surface.

Note that there are two distillation regions for this mixture—one large region shown as the red shaded region in Figure 2, and a second much smaller region shown as the unshaded region along the methanol–ethanol axis. These regions and their boundaries are a consequence of the azeotropes between methanol and acetone and ethanol and water. Note that the surface area of the boundary is clearly larger than the surface area generated by the interior collection of trajectories. Finally, it is important for the reader to understand that all trajectories in the larger distillation region start at the water vertex and end at the methanol–acetone azeotrope.

To generate trajectories and boundaries in four-component mixtures, different initial points on $B(x_0, \varepsilon)$ about the unstable water vertex were considered. This was accomplished using spherical coordinates and by choosing two different values of the angles, θ_1 and θ_2, which define a point on a sphere of radius ε about the unstable water vertex. Here θ_1 is the azimuthal angle while θ_2 is the polar angle as shown in Figure 2. These angles were then parameterized in the variables z_1 and z_2, respectively. The relationship between the angles and their parameterizations are given by the following equations.

$$\theta_1 = (\pi/2)z_1 \tag{8}$$

$$\theta_2 = (\pi/2)z_2 \tag{9}$$

To cover any potential ε-sphere, both θ_1 and θ_2 are allowed to vary from 0 to 2π (z_1 and z_2 from 0 to 4). However, for some unstable nodes, there are often additional restrictions that must be imposed so that only points on $B(x_0, \varepsilon)$ that lie within the feasible tetrahedron are considered. Table 1 lists the limits for each vertex of the tetrahedron in Cartesian coordinates. Other restrictions can exist when the unstable node is an azeotrope and are easily deduced.

The $c - 1$ initial conditions for Eq. 3 that lie on the ε-sphere about any unstable node are conveniently determined by converting from spherical to Cartesian coordinates using the equations,

$$x_1(0) = x_{10} + \varepsilon\cos\theta_1\sin\theta_2 \tag{10}$$

$$x_2(0) = x_{20} + \varepsilon\sin\theta_1\sin\theta_2 \tag{11}$$

$$x_3(0) = x_{30} + \varepsilon\cos\theta_2 \tag{12}$$

where x_{10}, x_{20}, and x_{30} denote the Cartesian coordinates of the unstable vertex.

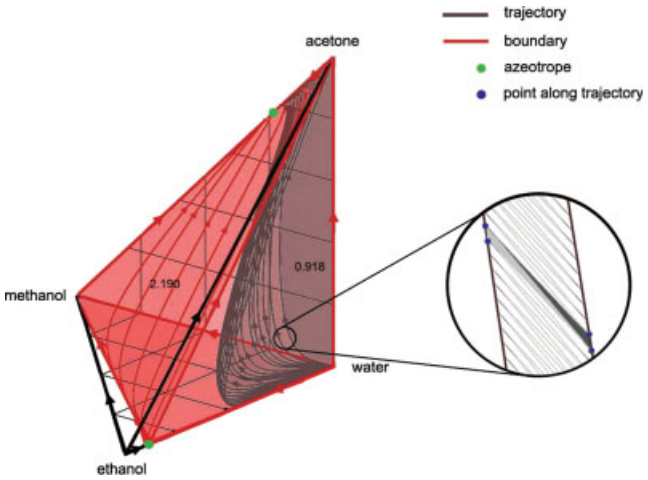

Figure 3. Calculation of surface areas using triangulation between trajectories.

[Color figure can be viewed in the online issue, which is available at www.interscience.wiley.com.]

Calculating Surface Areas by Triangulation

In order to show that maximum surface areas define separation boundaries for four-component mixtures that divide the tetrahedron into distinct distillation regions, surface areas must be calculated. Since each trajectory is made up of a series of discrete points, points on adjacent trajectories can be conveniently connected to form a series of triangles. These triangles can be used to compute the area between adjacent pairs of trajectories, as shown in Figure 3. That is, each time a step is taken in either trajectory, the area of the appropriate triangle is calculated. The lengths of the sides of the triangles are calculated by

$$L = [(x_1 - x_2)^2 + (y_1 - y_2)^2 + (z_1 - z_2)^2]^{1/2} \qquad (13)$$

where L is the length between points, and where one of the points is denoted by the ordered triple (x_1, y_1, z_1), and the other point is denoted by the ordered triple (x_2, y_2, z_2). Heron's formula, which uses the fact that the three sides of a triangle are known, is used to determine the area. Heron's formula states that

$$A = [s(s-a)(s-b)(s-c)]^{1/2} \qquad (14)$$

where A is the area, and a, b, and c denote the lengths of the sides of the triangle, and s is the semiperimeter given by

$$s = (a+b+c)/2 \qquad (15)$$

These areas were summed over the lengths of the two adjacent trajectories. Once the area between the two neighboring trajectories is calculated, the process is repeated for the next pair of neighboring trajectories until the areas between all trajectories that define the surface are calculated.

Before calculating surface areas of irregular shapes, the triangulation procedure just described was tested by computing the area of the triangle in Figure 3 defined by the ethanol–water azeotrope, the acetone vertex, and water vertex. The analytical surface area was calculated to be 0.4437. Using our numerical procedure and residue curves that *cover* the entire given triangular shape, the surface area was computed to be 0.4446 and gave a reasonable match to the analytical surface area.

Figure 3 also shows that while the system methanol/ethanol/acetone/water can have surfaces that are irregular, only one of these surface areas corresponds to the boundary. Boundaries and other shapes generated by families of trajectories, such as the regions shown in Figure 3, can be comprised of portions of triangular faces plus portions that are interior to the tetrahedron. To calculate surface areas we must therefore calculate surface areas on faces of the tetrahedron as well as surface areas of interior parts of the tetrahedron. To do this, we select an unstable node, generate pairs of trajectories—whether they lie in a face or the interior—and calculate areas by the numerical procedure described earlier.

As an example, consider Figure 3, in which there are two azeotropes—a methanol–acetone azeotrope and an ethanol–water azeotrope. The exact composition and temperature of these azeotropes are listed in Table 2. Note that the ethanol–water azeotrope divides the acetone/ethanol/water face and the methanol/ethanol/water face into two distillation regions each.

To illustrate how we determine a boundary in this four-component mixture, consider the water vertex and the methanol–acetone azeotrope, which are unstable (x_0) and stable nodes (x_T), respectively, with respect to Eq. 3. In this case, θ_1 and θ_2 are permitted to vary from 0 to $\pi/2$. We begin by fixing $\theta_1 = \pi/2$ such that it is in the ethanol/acetone/water face. We then determine the trajectory that has the longest line integral or distance with respect to θ_2 (or α_2) using Eqs. 3–5 for fixed θ_1 (or α_1). This gives a trajectory $x^*(\alpha_1, \alpha_2)_1$ and defines a point, $(\theta_1, \theta_2^*)_1$, on $B(x_0, \varepsilon)$. Next we rotate θ_1 by a small amount $-\Delta\theta_1$ and repeat the procedure of finding the longest trajectory using the procedure of Lucia and Taylor, and in doing so determine $x^*(\alpha_1, \alpha_2)_2$ and $(\theta_1, \theta_2^*)_2$. We caution the reader not to assume that this second (or any other subsequent) trajectory is restricted to some subspace; it is not! It will generally lie in the feasible tetrahedron embedded in R^3. We then calculate the area between these two adjacent trajectories of maximum distance. Finally, we repeat this procedure of continuously moving θ_1 by a small amount $-\Delta\theta_1$, finding the longest trajectory each time using the procedure of Lucia and Taylor, calculating the area between adjacent trajectories of maximum distance, and storing $x^*(\alpha_1, \alpha_2)_k$ and $(\theta_1, \theta_2^*)_k$ until we reach the methanol/acetone/water face. Figure 4 and Table 3 show numerical results for a set of trajectories for five different values of θ_1.

Note that in this example $\theta_2^* = 1.570796 = \pi/2$ for all values of θ_1 shown in Table 3. However, there is sensitivity to initial conditions, since small differences in θ_1 give very

Table 2. Azeotropes for the Methanol/Ethanol/Acetone/Water System

Azeotrope	Mole Fraction	Temperature (K)
Methanol–acetone	(0.2343, 0.7657)	329.736
Ethanol–water	(0.8874, 0.1126)	352.186

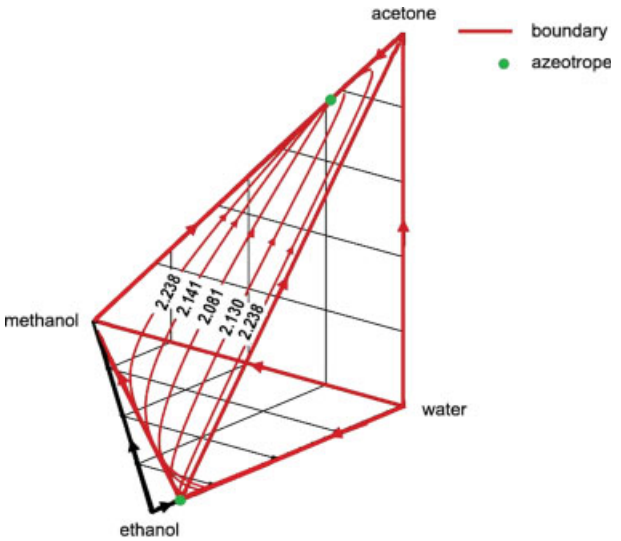

Figure 4. Trajectories of maximum distance on distillation boundary.

[Color figure can be viewed in the online issue, which is available at www.interscience.wiley.com.]

different trajectories and distances along the ethanol–water axis and the left face of the boundary shown in Figure 4. Moreover, small changes in θ_2 give very different line integral values or distances as well.

When we determine a sequence of points $\{(\theta_1, \theta_2^*)_k\}$ in this manner, we generate a function or curve $\theta_2^*(\theta_1)$ on $B(x_0, \varepsilon)$ in the form of a set of discrete points. Summing the areas as we go gives the surface area of the red shaded region in Figures 2 and 3. This surface area, which in this case has a value of 2.1898, is a maximum in surface area (as described in the next section) because it is comprised of a family of trajectories of maximum distance over the entire range of the angle θ_1. Note in this example that the boundary is an interior or embedded tetrahedron. Table 4 gives the numerical areas of each of the faces as well as the interior portion of this interior tetrahedron.

Levi-Civita Parallelism and Interior Shapes

A second interior shape was also generated to show that its surface area is indeed smaller than the surface area of the boundary. However, it is important to make clear to the reader what constitutes a meaningful comparison of surface areas and the method by which interior shapes are generated. The geometric basis for comparing surface areas in four-component mixtures is Levi-Civita parallelism.[21]

Table 3. Maximum Distances for Several Trajectories Along Distillation Boundary†

Starting Node	Ending Node	θ_1	θ_2^*	Distance
(0, 0, 0)	(0.234, 0, 0.766)	1.569225	1.570796	2.237856
(0, 0, 0)	(0.234, 0, 0.766)	1.566869	1.570796	2.130429
(0, 0, 0)	(0.234, 0, 0.766)	1.562942	1.570796	2.081122
(0, 0, 0)	(0.234, 0, 0.766)	1.559801	1.570796	2.140645
(0, 0, 0)	(0.234, 0, 0.766)	1.556659	1.570796	2.238481

†Component order is methanol(1), ethanol(2), acetone(3), water(4).

Table 4. Side Lengths and Corresponding Areas of the Interior Tetrahedron

Face	Side 1	Side 2	Hypotenuse	Area
Methanol/acetone/water	1.0000	1.0000	1.4142	0.5000
Ethanol/acetone/water	0.8874	1.0000	1.3370	0.4437
Methanol/ethanol/water	0.8874	1.0000	1.3370	0.4437
	Side 1	Side 2	Side 3	
Methanol/ethanol/acetone	1.4142	1.3370	1.3370	0.8023
			Total Area	*2.1898*

Formally, Levi-Civita parallelism requires some understanding of geodesics, acceleration along parameterized curves, and covariant derivatives. Intuitively, Levi-Civita parallelism is a way defining what it means to be parallel on a curved surface. Think of it this way. In Euclidean geometry, a line parallel to a given line in R^2 can be constructed by adding a vector of constant magnitude and direction to each point on that given line. The same is actually true for a smooth nonlinear curve embedded in R^2, and these concepts easily generalize to hyperplanes or surfaces embedded in R^n. Levi-Civita parallelism, on the other hand, is the non-Euclidean equivalent of parallelism in Euclidean spaces and its relevance to generating surfaces that do or do not describe distillation boundaries for four-component mixtures is tied to the fact that the set of initial conditions that define the boundary can be represented by the parameterized curve $\theta_2^*(\theta_1)$ on the surface $B(x_0, \varepsilon)$, where $B(x_0, \varepsilon)$ is a curved surface. Thus parallel on $B(x_0, \varepsilon)$ is not the same as parallel in R^3.

Figure 5 gives an illustration of Levi-Civita or parallel transport in the context of computing distillation boundaries in four-component mixtures. The lower curve in Figure 5, denoted by $\theta_2^*(\theta_1)$, is a smooth curve and consists of a set of initial conditions that define a distillation boundary. The curve $\theta_2^*(\theta_1)$ is not necessarily a line of constant latitude, but it does intersect many lines of constant longitude or meridians on $B(x_0, \varepsilon)$. Thus, each point on $\theta_2^*(\theta_1)$ on $B(x_0, \varepsilon)$ is also a point on some meridian. Since these lines of constant longitude are portions of great circles, they are also geodesics on $B(x_0, \varepsilon)$. As a result, they are tangent to $\theta_2^*(\theta_1)$ and have zero acceleration. To each point on $\theta_2^*(\theta_1)$ on $B(x_0, \varepsilon)$ we add a small but fixed portion of the appropriate meridian. Note that this is easily accomplished in spherical coordinates by moving each point on $\theta_2^*(\theta_1)$ a small but fixed amount, say $\Delta\theta_2$, along each meridian. Tangent to each

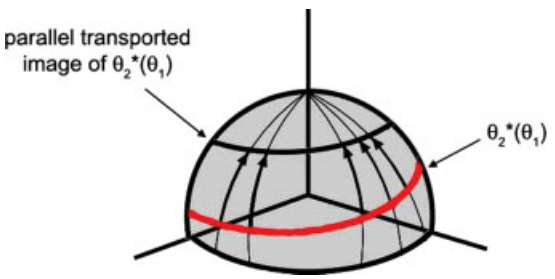

Figure 5. Parallel transport of $\theta_2^*(\theta_1)$ that defines boundary.

[Color figure can be viewed in the online issue, which is available at www.interscience.wiley.com.]

Table 5. Comparison of Areas Between Interior Shape and Boundary Surface

Side	Irregular Shape	Interior Tetrahedron
Ethanol/acetone/water	0.3034	0.4437
Methanol/acetone/water	0.1681	0.5000
Interior surface	0.4463	1.2461
Total area	*0.9179*	*2.1898*

meridian is a velocity vector, and since movement along any velocity vector for a line of constant longitude has zero acceleration, the covariant derivative of that velocity vector is also zero. Consequently, the collection of velocity vectors on $\theta_2^*(\theta_1)$ or velocity vector field defined in this manner is Levi-Civita parallel.[21] Basically, all we are doing here is moving each point on $\theta_2^*(\theta_1)$ due north on $B(x_0, \varepsilon)$.

The result of this deliberate construction is that the upper curve shown in Figure 5, which defines a different set of initial conditions than those that define the distillation boundary, is parallel to $\theta_2^*(\theta_1)$ on $B(x_0, \varepsilon)$. Of course, care must be taken to make sure that one moves along lines of constant longitude on $B(x_0, \varepsilon)$ in the "correct direction" so that the resulting set of initial conditions is both physically meaningful and converges to the same stable node.

Remark

The reason Levi-Civita parallelism is required is because one could easy construct surfaces interior to any distillation boundary with many peaks and valleys that would have surface areas far greater than that of the boundary. However, if Levi-Civita parallelism is imposed, then the distillation boundary must have the largest local surface area. Again, note also that parallel transport is easily accomplished in spherical coordinates by simply changing θ_2 (or z_2 in Eq. 9). Table 5 gives a comparison of the areas that make up the boundary surface and the interior balloon.

Optimization Formulation and Equations

The correct optimization formulation for finding distillation boundaries in quaternary mixtures consists of solving a collection of nonlinear programming problems defined by

$$\max_{x(0)} D = \int_0^T \left\| x'(\alpha) \right\| d\alpha \tag{16}$$

$$\text{subject to} \quad x'(\alpha) = y[x'(\alpha)] - x(\alpha) \tag{17}$$

$$x(T) = x_T \tag{18}$$

over a sequence of fixed values $\{\theta_1\}$, where it is understood that θ_1 and θ_2 determine initial conditions for Eq. 17 and that we seek the value of θ_2^* that maximizes D. Thus for each value of θ_1 we find $\theta_2^*(\theta_1)$ that gives the longest line integral. It is in this way, and under the imposition of Levi-Civita parallelism, that a collection of trajectories that satisfy Eqs. 16–18 represent a local maximum in surface area described by the problem given in the introduction (i.e., Eqs. 2–4) and define a distillation boundary in four-component mixtures. Note that any distillation boundary will consist of a set of trajectories, say $x^*(\alpha_1, \alpha_2)_k$, for $k = 1, \ldots, N$, where N is simply some integer value.

Numerical Results

In this section, numerical results are presented to show that distillation boundaries in four-component mixtures correspond to local maxima in surface areas as described in previous sections of this paper. In all examples in this section, the liquid phase was modeled using the UNIQUAC equation of Prausnitz et al.,[22] while the vapor phase was assumed to be ideal unless specified otherwise. All trajectories defined by Eq. 17 were integrated using a simple forward Euler method with a fixed step size of $h = 10^{-2}$ for 30,000 steps to ensure convergence to a stable node—even though convergence was often obtained in far fewer than 30,000 steps. Any compositions that were determined to be zero were reset to 10^{-25} and a radius of $\varepsilon = 10^{-3}$ was used for $B(x_0, \varepsilon)$ in all examples. All numerical computations were performed on both a Pentium IV computer using the Lahey-Fijitsui LF95 compiler and a Pentium III computer using the Lahey F77-EM32 compiler.

Example 1: Acetic Acid(1)/Ethanol(2)/Ethyl Acetate(3)/Water(4)

The purpose of this example is to show that when there are no distillation boundaries the procedure described in the previous section simply computes the surface area of the tetrahedral feasible region. Here the vapor phase is modeled using the Hayden-O'Connell equation to account for dimerization of carboxylic acids.

This mixture has two binary and one ternary azeotrope restricted to the ethanol/ethyl acetate/water face. The azeotropic compositions and temperatures are shown in Table 6. Figure 6, on the other hand, shows the behavior of residue curves for this mixture. Note that all residue curves begin in the acetic acid corner—since acetic acid is the high boiler—and end at the ternary ethanol–ethyl acetate–water azeotrope. Thus the unstable node is $x_0 = (0, 0, 0)$ while the stable node is $x_T = (0.1351, 0.5546, 0.3103)$. However, it is important to point out that even though there are no distillation boundaries that are interior to the feasible tetrahedral region, trajectories can still have rather complicated behavior. For example, the trajectory with the distance of 1.364 appears to loop into the stable node while others—the one with the distance 2.406—can follow a rather circuitous path to the stable node. Clearly, the trajectories in Figure 6 show that

Table 6. Azeotropes for the Ethanol/Ethyl Acetate/Acetic Acid/Water

Azeotrope	Mole Fraction	Temperature (K)
Ethyl acetate–water	(0.6182, 0.3818)	344.189
Ethyl acetate–ethanol	(0.5365, 0.4635)	345.946
Ethanol–ethyl acetate–water	(0.1351, 0.5546, 0.3103)	343.902

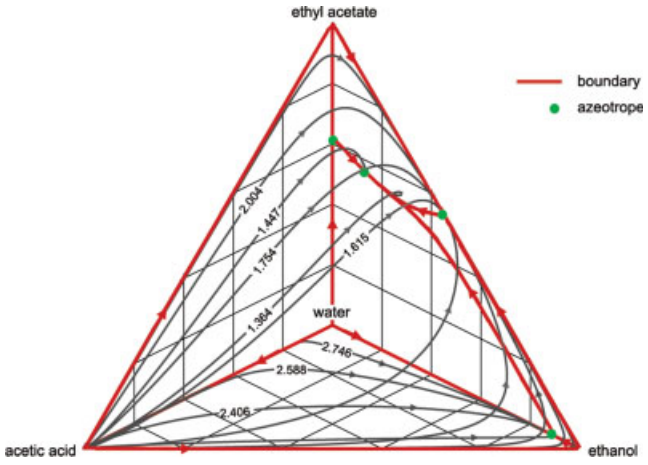

Figure 6. Residue curves and line integrals for acetic acid/ethanol/ethyl acetate/water.

[Color figure can be viewed in the online issue, which is available at www.interscience.wiley.com.]

there are no internal distillation boundaries. Moreover, the longest paths are those that first trace the perimeters of the appropriate triangular faces before entering the ethanol/ethyl acetate/water face, and there are also locally longest paths internal to the ethanol/ethyl acetate/water face. All local maxima in distance are shown in red in Figure 6. As a consequence, the maximum surface area is unique and has a value of 2.23607—which is the surface area of an equilateral tetrahedron whose sides are of length 1.

Example 2: Methanol(1)/Ethanol(2)/ Acetone(3)/Water(4)

This second example, which was used in the illustration sections of this paper, is included here to demonstrate the fundamental geometric concepts associated with distillation boundaries in four-component mixtures. It is also an illustration of the simplest kind of distillation boundary—one that looks planar and divides the feasible tetrahedron into two distinct distillation regions. Here the vapor phase is assumed to be ideal.

In Figure 2 we showed that the surface area of the boundary for the larger distillation region was 2.1898. We also calculated the surface area of one interior shape, which had a surface area of 0.9179. The interior shape was generated by Levi-Civita parallel transport of $\theta_2^*(\theta_1)$ on $B(x_0, \varepsilon)$ and by sweeping through the range of θ_1 from 0 to $\pi/2$ in order to generate a number of trajectories. We note here that trajectories are very sensitive to initial conditions, and that the amount of parallel transport used to generate the interior surface was quite small. In particular, the distillation boundary shown in Figure 2 corresponds to $\theta_2^*(\theta_1) = (1 - 10^{-25})\pi/2$ or essentially $\pi/2$. On the other hand, only a small change of $\Delta\theta_2 = (1 - 10^{-9})\pi/2$ yields line integrals of significantly smaller distance and a resulting surface area under parallel transport of 0.9179. Figure 7, on the other hand, shows the trajectories that make up a second, larger interior shape with a surface area of 1.290. While this second interior shape is larger than the one shown in Figure 2, it is still contained within the distillation boundary described by a local maximum in surface area of 2.1898. This second interior shape was generated by *less* parallel transport of $\theta_2^*(\theta_1)$ on $B(x_0, \varepsilon)$. The two interior shapes in Figures 2 and 7, respectively, illustrate how sensitive these shapes are to initial conditions. Finally, the maximum surface area of the second smaller distillation region in Figure 7 is 1.7809 and was computed in exactly the same way as the larger surface area by starting at the unstable ethanol vertex.

Example 3: Chloroform(1)/Methanol(2)/ Acetone(3)/Water(4)

This final example in this article is an illustration of a quaternary mixture at atmospheric pressure that gives rise to more complex distillation boundary structure. There are four binary azeotropes and two ternary azeotropes in this system, and these azeotropes result in highly curved and interesting boundaries that divide the feasible tetrahedron into four distinct distillation regions. Table 7 summarizes the composition and temperature of all azeotropes of this mixture.

Figure 8 shows the distillation boundaries, maximum surfaces areas, and various trajectories on those boundaries for the chloroform/methanol/acetone/water mixture. For clarity, we have left the portions of any triangular face of any distillation region unshaded and have shaded only the interior portions of the distillation boundaries. Table 8, on the other hand, gives the local maxima in surface area for each of the four distinct distillation regions. We note that the surface areas reported in Figure 8 and Table 8 do, in fact, include the areas of the interior boundaries as well as the appropriate triangular faces. Since there are four distinct regions, four separate pairs of unstable and stable nodes were required to generate the geometric shapes in Figure 8. For example, for the distillation region in the chloroform corner, the unstable node is the chloroform–acetone azeotrope while the stable node is the chloroform–water azeotrope.

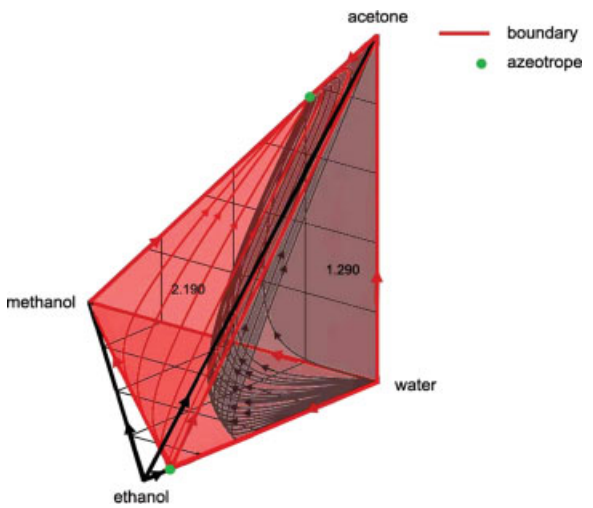

Figure 7. Surface areas and distillation boundary for methanol/ethanol/acetone/water.

[Color figure can be viewed in the online issue, which is available at www.interscience.wiley.com.]

Table 7. Azeotropes for Chloroform/Methanol/Acetone/Water

Azeotrope	Mole Fraction	Temperature (K)
Methanol–acetone	(0.2343, 0.7657)	329.736
Chloroform–methanol	(0.6531, 0.3469)	327.517
Chloroform–acetone	(0.6414, 0.3586)	339.121
Chloroform–methanol–acetone	(0.2173, 0.4470, 0.3357)	330.65
Chloroform–water	(0.7891, 0.2109)	327.486
Chloroform–acetone–water	(0.3326, 0.4836, 0.1838)	333.55

As in example 2, we made a comparison between the surface area of the distillation boundary and the surface area of a shape contained within that boundary under Levi-Civita parallelism. Figure 9 shows this comparison for the distillation region in the chloroform corner and is highlighted in red. More specifically, this distillation region has a maximum surface area of 0.7907. Note that the smaller shape is completely contained within this region and clearly has a smaller surface area of 0.3793. Table 9 compares the surface areas of the interior shape to the surface area of the boundary by parts and as a whole.

Conclusions

The geometric notion of surface areas in Lucia and Taylor[6] was developed rigorously to show that distillation boundaries in quaternary mixtures are defined by local maxima in surface areas under the condition of Levi-Civita parallelism. A triangulation technique for calculating surface areas and a straightforward and implementable optimization methodology for actually computing distillation boundaries were described. The optimization approach that was presented makes use of repeated maximum line integral computations to find local maxima surface areas. Several numerical examples were presented to demonstrate a wide variety of distillation boundaries encountered in four-component systems and to show that distillation boundaries in four-component mixtures are local maxima in surface areas.

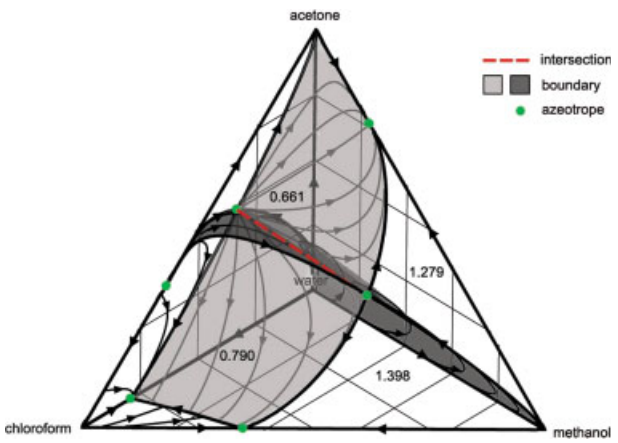

Figure 8. Distillation boundaries for chloroform/methanol/acetone/water.

[Color figure can be viewed in the online issue, which is available at www.interscience.wiley.com.]

Table 8. Maximum Surface Areas of Regions for the Chloroform/Methanol/Acetone/Water System

Region	Surface Area
Chloroform corner	0.790
Lower methanol/water corner	1.398
Upper methanol/water corner	1.279
Acetone corner	0.661

Finally, the concepts developed in this article can be used to determine distillation boundaries for mixtures with five or more components, where full visualization is not possible. The algebraic formulation of the corresponding optimization problem is very similar to that defined by Eqs. 2–4. More specifically, the optimization formulation for distillation boundaries in systems with five or more components is given by

$$\max_{x(0)} V = \int\int \dots \int [x'(\alpha_1, \alpha_2, \dots, \alpha_{c-1})] d\alpha_1 \, d\alpha_2 \dots d\alpha_{c-1} \tag{19}$$

$$\text{subject to} \quad x'(\alpha_1, \alpha_2, \dots, \alpha_{c-1}) = y[x'(\alpha_1, \alpha_2, \dots, \alpha_{c-1})] - x(\alpha_1, \alpha_2, \dots, \alpha_{c-1}) \tag{20}$$

$$x(T) = x_T \tag{21}$$

where V is the volume or hypervolume, $x(\alpha_1,\alpha_2, \dots, \alpha_{c-1})$ is parameterization of any trajectory over the domain of interest, and all other quantities are defined as earlier. In addition, Levi-Civita parallelism must be used to make meaningful comparisons of volumes, so that one can make the strong statement that the resulting set of trajectories $\{x^*(\alpha_1, \alpha_2, \dots, \alpha_{c-1})_k\}$, for $k = 1, \dots, N$ generate a local maximum in vol-

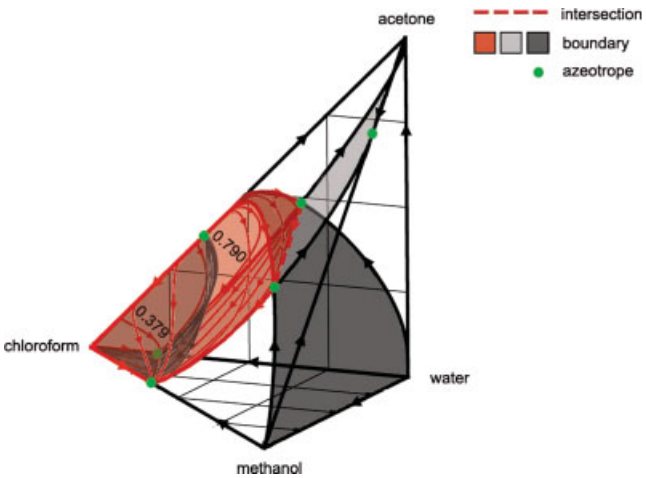

Figure 9. Boundary and interior surface areas for methanol/ethanol/acetone/water.

[Color figure can be viewed in the online issue, which is available at www.interscience.wiley.com.]

Table 9. Comparison of Surface Areas Between Interior Shape and Boundary

Side	Irregular Shape	Boundary Surface
Chloroform/acetone/water	0.0584	0.1047
Chloroform/methanol/water	0.0366	0.0366
Chloroform/methanol/acetone	0.1623	0.3246
Interior surface	0.1220	0.2738
Total area	*0.3793*	*0.7907*

ume and define a distillation boundary. Note, however, that there is a combinatorial aspect to any implementation based on this optimization approach as the number of components increases. For example, for a five-component mixture it is necessary to find families of local maxima in surface area over a span of angles θ_3 and those local maxima in surface area require families of local maxima in distance to be determined over a span of angles θ_2. Thus for a five-component system using a uniform grid in rotation angles requiring n grid points, n^2 optimization problems must be solved and, in general, the number of optimizations required for a c-component mixture is n^{c-3}.

Acknowledgments

A. Lucia thanks the National Science Foundation for support of this work under Grant No. CTS-0624889.

Literature Cited

1. Ostwald W. Dampfdrucke ternarer gemische. Abahndlungen der Mathematisch-Physischen der Konig Sachsischen. *Gesellschaft Wissenschaften*. 1900;25:413.
2. Ostwald W. *Lehrbuk der Allgemeinen Chemie*. Leipzig, Germany: Engelmann, 1902.
3. Schreinemakers FAH. Dampfdrucke ternarer gemische. I. Theoretischer teil. *Z Phys Chem*. 1901;36:257–289.
4. Schreinemakers FAH. Dampfdrucke ternarer gemische. II. Theoretischer teil. *Z Phys Chem*. 1901;36:413–449.
5. Schreinemakers FAH. Dampfdrucke ternarer gemische. III. Theoretischer teil. *Z Phys Chem*. 1901;36:710–740.
6. Lucia A, Taylor R. The geometry of separation boundaries. I. Basic theory and numerical support. *AIChE J*. 2006;52:582–594.
7. Kiva VN, Hilmen EK, Skogestad S. Azeotropic phase equilibrium diagrams: a survey. *Chem Eng Sci*. 2003;58:1903–1953.
8. Doherty MF, Perkins JD. On the dynamics of distillation processes. I. The simple distillation of multicomponent, nonreacting, homogeneous mixtures. *Chem Eng Sci*. 1978;33:281–301.
9. Doherty MF, Perkins JD. On the dynamics of distillation processes. III. The topological structure of ternary residue curve maps. *Chem Eng Sci*. 1979;34:1401–1414.
10. Pham HN, Doherty MF. Design and synthesis of heterogeneous azeotropic distillations. I. Heterogeneous phase diagrams. *Chem Eng Sci*. 1990;45:1823–1836.
11. Pham HN, Doherty MF. Design and synthesis of heterogeneous azeotropic distillations. II. Residue curve maps. *Chem Eng Sci*. 1990;45:1837–1844.
12. Barbosa D. Doherty MF. The influence of chemical reactions on vapor–liquid phase diagrams. *Chem Eng Sci*. 1988;45:529–540.
13. Barbosa D, Doherty MF. The simple distillation of homogeneous reactive mixture. *Chem Eng Sci*. 1988;43:541–550.
14. Barbosa D, Doherty MF. Design and minimum reflux calculations for single-feed multicomponent reactive distillation columns. *Chem Eng Sci*. 1988;43:1523–1537.
15. Van Dongen DB, Doherty MF. On the dynamics of distillation processes vs. the topology of the boiling temperature surface and its relation to azeotropic distillation. *Chem Eng Sci*. 1984;39:883–892.
16. Foucher ER, Doherty MF, Malone MF. Automatic screening of entrainers for homogeneous azeotropic distillation. *Ind Eng Chem Res*. 1991;29:760–772.
17. Peterson EJ, Partin LR. Temperature sequences for categorizing all ternary distillation boundary maps. *Ind Eng Chem Res*. 1997;36:1799–1811.
18. Rooks RE, Julka V, Doherty MF, Malone MF. Structures of distillation regions for multicomponent azeotropic mixtures. *AIChE J*. 1988;44:1382–1391.
19. Krolikowski LJ. Determination of distillation regions for non-ideal ternary mixtures. *AIChE J*. 2005;52:532–544.
20. Pöpken T, Gmehling J. Simple method for determining the location of distillation region boundaries in quaternary systems. *Ind Eng Chem Res*. 2004;43:777–783.
21. Thorpe, JA. *Elementary Topics in Differential Geometry*. Springer-Verlag: New York, 45–47
22. Prausnitz JM, Anderson TF, Grens EA, Eckert CA, Hsieh R, O'Connell JP. *Computer Calculations for Multicomponent Vapor–Liquid and Liquid–Liquid Equilibria*. Engelwood Cliffs: Prentice-Hall, 1980.

Manuscript received Sept. 14, 2006, and revision received Mar. 30, 2007.